Zero-helicity Lagrangian kinematics of three-dimensional advection

Darryl D. Holm and Yoshifumi Kimura
Theoretical Division and Center for Nonlinear Studies, Los Alamos National Laboratory, MS B284, Los Alamos, New Mexico 87545

(Received 12 October 1990; accepted 24 January 1991)

The toroidal–poloidal decomposition for divergenceless vector fields in three dimensions is used to classify incompressible steady velocity fields in three dimensions according to whether they have zero, or nonzero helicity, and whether they are integrable, or nonintegrable as dynamical systems. Linearized steady Rayleigh–Bénard convection flows provide examples from each class. Computational techniques that preserve volume and helicity are developed and used to visualize the Lagrangian particle trajectories of three-dimensional advection for two Rayleigh–Bénard flows having zero helicity in a periodic domain.

I. INTRODUCTION

The Lagrangian representation of the motion of a fluid particle path $\mathbf{x}(t)$ in a steady incompressible flow in $\mathbb{R}^3$ is given by the dynamical system of advection equations $\dot{\mathbf{x}} = \mathbf{v}(\mathbf{x})$, with $\operatorname{div} \mathbf{v} = 0$. When $\mathbf{v}$ is a nonlinear function of $\mathbf{x}$, dynamical systems theory implies that the solutions of these advection equations may exhibit deterministic chaos (e.g., show extreme sensitivity to initial conditions), even though the function $\mathbf{v}$ is smooth. In such cases, fluid particle paths that start close to one another generally do not stay close, even in stable "laminar" flows. Regarding the advection equations as a dynamical system [i.e., a mechanical system with degrees of freedom $\mathbf{x}(t)$] thus raises the issue of distinguishing among fluid flows on the basis of whether their Lagrangian particle paths are regular or chaotic. As a dynamical systems question, the issue is to decide on the integrability of a given advection equation. For the present purposes, a dynamical system in $\mathbb{R}^3$ is said to be "integrable" if its orbits can be reduced to a "phase portrait," i.e., a parametrized set of non-self-intersecting curves on a two-dimensional manifold. Of course, this issue also arises in many other fields and has been widely investigated, particularly in studies of geometrical configurations of magnetic field lines. These magnetic-field-line studies indicate that nonintegrable divergenceless flows in $\mathbb{R}^3$ may have dense, space-filling orbits and may show extreme sensitivity to initial conditions, leading to a loss of predictability, even though the system is deterministic. In contrast, integrable divergenceless flows in $\mathbb{R}^3$ have only periodic and homoclinic (or heteroclinic) orbits, whose behavior is regular and does not lose predictability over time.

Three-dimensional incompressible flows possess a property not possessed by planar flows called "helicity," which indicates the linkage, or knottedness of the flow. This, in turn, indicates the complexity of the flow, and may also indicate something about its mixing properties. The helicity of an incompressible flow $\mathbf{v}$ with vorticity $\boldsymbol{\omega} = \operatorname{curl} \mathbf{v}$ in a three-dimensional domain Ω is given by the integral over the domain of flow, $\Lambda = \int_\Omega \mathbf{v}\cdot\boldsymbol{\omega}$. The helicity measures the total number of (positive and negative) links, or knots, of the velocity field $\mathbf{v}$ with itself. See Arnold[1–3] for a discussion of the significance of helicity as a topological property, which is *invariant* under volume-preserving diffeomorphisms.

The helicity is of interest here, because nonzero helicity is a necessary condition for nonintegrable particle motion (see Arnold[1] and Hénon[4]). Nonintegrable particle motion includes, but is not limited to, chaotic particle paths (streaklines).

The aim of the present work is to look further at integrable and nonintegrable particle motion for three-dimensional incompressible flows whose helicity is *zero*. This is done on the grounds that zero-helicity flows in three dimensions might be expected to be less complex (and, therefore, more tractable) than flows with nonzero helicity. To visualize these flows, we develop a numerical integration technique that models volume-preserving diffeomorphisms (and thereby preserves helicity) to high accuracy.

Two zero-helicity flows derived from the linearized steady Rayleigh–Bénard convection equations are modeled in detail. Both flows possess saddle-focus connections, and both are deformations of the same basic integrable flow. That is, these two flows both limit to the same basic integrable flow when certain parameters in the equations are set to zero. One of these flows—of Chandrasekhar[5]—is an integrable deformation of the basic integrable flow, while the other—of Arter[6]—is a nonintegrable deformation of the same integrable flow. (The Arter flow is a sum of two integrable Hamiltonian flows in $\mathbb{R}^3$ that is not integrable in general.)

Even for these relatively simple cases, computer simulations indicate that great care must be exercised in modeling three-dimensional (3-D) flows to avoid producing chaotic behavior as a numerical artifact. In particular, the spatially periodic heteroclinic network of saddle-focus connections, which is present analytically in the integrable Chandrasekhar flow, is found in the numerical integrations to show twisted, ribbonlike structures with intricate geometrical patterns. These geometrical patterns are due to phase relations imposed on nearly recurrent orbits by preservation of volume in the numerical algorithm. However, the orbits should be exactly recurrent, i.e., periodic. Instead, perturbations (caused by small numerical errors) are amplified in passing repeatedly through the network of spiral foci in the Chandrasekhar flow, and these perturbations apparently lead to Shilnikov chaos. (The saddle foci of the heteroclinic network do satisfy the Shilnikov criterion for a perturbed heteroclinic cycle to produce sensitive dependence on initial

Downloaded 07 Jan 2004 to 128.165.156.80. Redistribution subject to AIP license or copyright, see http://ojps.aip.org/phf/phfcr.jsp

conditions. However, the presence of Shilnikov chaos is not rigorously demonstrated here for the numerical algorithm we use.)

The next section divides three-dimensional incompressible flows into classes, according to their helicity and their integrability as dynamical systems. The classes are zero helicity, or nonzero helicity: integrable, or nonintegrable. These classes of flows are delineated using the two scalar potentials in the well-known toroidal–poloidal decomposition for divergenceless vector fields in $\mathbb{R}^3$. Linearized steady Rayleigh–Bénard convection flows provide examples from each class. In Sec. III, computational techniques for modeling volume-preserving diffeomorphisms (and, hence, preserving helicity) are developed, and used to visualize the Lagrangian particle trajectories of three-dimensional advection for two zero-helicity flows, the (nonintegrable) Arter flow and the (integrable) Chandrasekhar flow, for various values of the parameters in these flows.

II. CLASSIFICATION OF 3-D FLOWS

A. Toroidal–poloidal decomposition

Steady three-dimensional incompressible velocity fields may be represented by the well-known toroidal–poloidal (T–P) decomposition,

$$\mathbf{v} = \operatorname{curl}(G\hat{\mathbf{z}}) + \operatorname{curl}\operatorname{curl}(H\hat{\mathbf{z}}), \tag{1}$$

where G and H are the toroidal and poloidal scalar potentials, respectively, and $\hat{\mathbf{z}} = \nabla z$ is the unit vector in the z direction. (See, e.g., Chandrasekhar *et al.*[7–9] for discussions of the T–P decomposition.) The functions G and H are related to the z components of vorticity and fluid velocity by

$$\begin{aligned} \Delta_\perp G &= -(\operatorname{curl}\mathbf{v}\cdot\hat{\mathbf{z}}) = -(\boldsymbol{\omega}\cdot\hat{\mathbf{z}}), \\ \Delta_\perp H &= -(\mathbf{v}\cdot\hat{\mathbf{z}}), \end{aligned} \tag{2}$$

where $\Delta_\perp = \partial_{xx} + \partial_{yy}$ is the Laplacian operator in the horizontal plane. The velocity in the T–P decomposition is invariant under the following gauge transformation:

$$H \to H' = H + \eta, \quad G \to G' = G + \gamma,$$

where η and γ satisfy

$$\gamma\hat{\mathbf{z}} + \operatorname{curl}\eta\hat{\mathbf{z}} = \nabla\varphi,$$

for some continuous function φ, defined on $\mathbb{R}^3$. Hence the T–P decomposition is not unique, but has an additive degree of gauge freedom. The T–P potentials G and H are analogs for fluid flows in three dimensions of the streamfunction and velocity potential in two dimensions. The T–P decomposition itself is akin to the complex streamfunction representation of planar incompressible flows. This can be seen by looking at the T–P decomposition in components,

$$\mathbf{v} = \begin{pmatrix} G_{,y} + H_{,xz} \\ -G_{,x} + H_{,yz} \\ -\Delta_\perp H \end{pmatrix}. \tag{3}$$

So G is the analog of the streamfunction in two dimensions, and $H_{,z}$ is the analog of the velocity potential. Just as in the planar case, the horizontal velocity components are Cauchy–Riemann expressions, so flows with nonzero velocity may be associated to *singular* complex functions. The gauge freedom in the T–P decomposition corresponds to adding an analytic function of the variable $x + iy$ to the complex sum $F = H_{,z} + iG$.

B. A Class of flows with nonzero helicity: Beltrami flows

Beltrami flows are steady solutions of Euler equations that satisfy the relation $\operatorname{curl}\mathbf{v} = \lambda\mathbf{v}$ (where $\lambda = \text{const}$). That is, the velocity and vorticity are everywhere parallel, so the fluid particles move along their axis of rotation. Beltrami flows have nonzero helicity, $\Lambda \neq 0$, since $\mathbf{v}\cdot\boldsymbol{\omega} = \lambda v^2$ is of constant sign throughout the flow. Using the T–P decomposition (3) allows the Beltrami property to be written as

$$\begin{pmatrix} -\Delta H_{,y} + G_{,xz} \\ \Delta H_{,x} + G_{,yz} \\ -\Delta_\perp G \end{pmatrix} = \lambda \begin{pmatrix} G_{,y} + H_{,xz} \\ -G_{,x} + H_{,yz} \\ -\Delta_\perp H \end{pmatrix}, \tag{4}$$

where $\Delta = \partial_{xx} + \partial_{yy} + \partial_{zz}$. Relation (4) for Beltrami flows holds (up to gauge equivalence) when $G = \lambda H$ and $-\Delta H = \lambda^2 H$.

The ABC flow,[1,10]

$$\dot{x} = A\sin z + C\cos y, \quad \dot{y} = B\sin x + A\cos z, \quad \dot{z} = C\sin y + B\cos x, \tag{5}$$

provide an example of Beltrami flow, for which $\lambda = 1$ and $G = H = -Ax\cos z + B\cos x + C\sin y$, in the T–P decomposition. These flows are nonintegrable, except at isolated values of the parameters A, B, and C. (See Dombre *et al.*[10] for a clear treatment of ABC flows from a dynamical systems viewpoint, as well as a description of their applicability in fluid dynamics.)

C. Zero-helicity flows

The vector formulas for $\mathbf{v}$ and $\boldsymbol{\omega}$ from (3),

$$\begin{aligned} \mathbf{v} &= \nabla H_{,z} + \nabla G \times \hat{\mathbf{z}} - \Delta H\hat{\mathbf{z}}, \\ \boldsymbol{\omega} &= \nabla G_{,z} - \nabla\Delta H \times \hat{\mathbf{z}} - \Delta G\hat{\mathbf{z}}, \end{aligned} \tag{6}$$

provide the following expression for the helicity integrand $\mathbf{v}\cdot\boldsymbol{\omega}$, in terms of the T–P potentials:

$$\begin{aligned} \mathbf{v}\cdot\boldsymbol{\omega} = \hat{\mathbf{z}}\cdot[\nabla\Delta H \times \nabla H_{,z} + \nabla G_{,z} \times \nabla G] + \nabla_\perp G\cdot\nabla_\perp\Delta H \\ + (\nabla H_{,z} - \Delta H\hat{\mathbf{z}})\cdot(\nabla G_{,z} - \Delta G\hat{\mathbf{z}}). \end{aligned} \tag{7}$$

The volume integral of the first term in (7) vanishes for flows with periodic boundary conditions, and for flows vanishing at infinity. Upon assuming periodic boundary conditions, the remaining two terms in (7) vanish in one of the following three cases: (I) $G \neq 0$, $H = 0$; (II) $G = 0$, $H \neq 0$; or (III) $G = \mathbf{k}\nabla H$, $-\Delta H = \lambda^2 H$, where $\mathbf{k}$ is a constant vector. These three cases provide us with three categories of zero-helicity flows:

(I) $G \neq 0$, $H = 0$.

This first category consists of two-dimensional Hamiltonian flows, with G as the Hamiltonian. (Of course, G is also the streamfunction.) Plainly, these Hamiltonian flows have zero helicity, and (being two dimensional) they are integrable:

(II) $G = 0$, $H \neq 0$.

Arter[6] studies a flow in this second category. The Arter flow

Downloaded 07 Jan 2004 to 128.165.156.80. Redistribution subject to AIP license or copyright, see http://ojps.aip.org/phf/phfcr.jsp

is given by

$$\begin{aligned}\dot{x} &= -\sin x \cos y \cos z + b \sin 2x \cos 2z,\\ \dot{y} &= -\cos x \sin y \cos z + b \sin 2y \cos 2z,\\ \dot{z} &= 2 \cos x \cos y \sin z - b(\cos 2x + \cos 2y)\sin 2z,\\ H &= \cos x \cos y \sin z - \tfrac{1}{4}b(\cos 2x + \cos 2y)\sin 2z.\end{aligned} \tag{8}$$

This is a model flow with square planform for the onset of Rayleigh–Bénard convection. Expression (8) gives a flow that appears to be nonintegrable unless b either vanishes, or is infinite. (In the later case, time t must be rescaled to time $t' = bt$.) Numerical integrations are claimed in Ref. 6 to show the onset of chaos resulting from resonant island overlap, as b increases from zero to unity. Thus, although they do have zero helicity, the flows in this category would be expected in general to be nonintegrable unless H is separable in z, i.e., unless $H = f(x,y)g(z)$;

(III) $G = \mathbf{k}\cdot\nabla H$, $-\Delta H = \lambda^2 H$ ($\mathbf{k}$ is a constant vector).

A good example in this third category is a flow introduced by Veronis[11] and by Chandrasekhar[5] as a model for the onset of Rayleigh–Bénard convection with rotation,

$$\begin{aligned}\dot{x} &= -\sin x \cos y \cos z - K^2 \cos x \sin y \cos z,\\ \dot{y} &= -\cos x \sin y \cos z + K^2 \sin x \cos y \cos z,\\ \dot{z} &= 2 \cos x \cos y \sin z.\end{aligned} \tag{9}$$

This flow is derived as a lowest-mode linearized solution of the Navier–Stokes equations with buoyancy for a rotating fluid in a periodic cube (T^3) under the Boussinesq approximation. The parameter K is proportional to the rate of rotation around the z axis. The flow (9) is obtained in the T–P decomposition (1) by setting

$$H = \cos x \cos y \sin z \quad \text{and} \quad G = K^2 H_{,z}. \tag{10}$$

Remark: The Chandrasekhar flow in Eq. (9) can also be characterized as separable (in the z dependence of H with $G = K^2 H_{,z}$), which is also sufficient for T–P flows in (1) to be integrable. One may demonstrate this remark by regarding z as an independent variable in (9) and dividing the first and second equations by the third one. Hence

$$\begin{aligned}\frac{dx}{d(\log \sin z)} &= -\frac{1}{2}(\tan x + K^2 \tan y),\\ \frac{dy}{d(\log \sin z)} &= -\frac{1}{2}(\tan y - K^2 \tan x).\end{aligned} \tag{11}$$

These equations are expressible in two-dimensional vector form as

$$\begin{pmatrix} \dfrac{dx}{d\alpha} \\ \dfrac{dy}{d\alpha} \end{pmatrix} = \begin{pmatrix} 1 & K^2 \\ -K^2 & 1 \end{pmatrix} \begin{pmatrix} \partial_x \log\sqrt{\cos x \cos y} \\ \partial_y \log\sqrt{\cos x \cos y} \end{pmatrix}, \tag{12}$$

where $\alpha = \log \sin z$. Equation (12) shows the Chandrasekhar flow always has two-dimensional structure and, thus, is integrable in the variable z. In fact, the flow lines of (12) are *periodic*, except for heteroclinic orbits.

Remark: The Arter flow (8) with $b = 0$ coincides with the Chandrasekhar flow (9) when $K = 0$. This basic flow is expressible as

$$\dot{\mathbf{x}} = \nabla C_1 \times \nabla C_2, \tag{13}$$

where $C_1 = \log(\sin x/\sin y)$ and $C_2 = \sin x \sin y \sin z$ are two constants of the motion. Thus Eq. (13) is the "unperturbed version" of both the Arter flow (8) and the Chandrasekhar flow (9). Equation (13) implies that the flow takes place on intersections of the level surfaces of C_1 and C_2. This flow may be shown to be Hamiltonian and integrable, by defining a noncanonical Poisson bracket, namely $\{F, G\} = \nabla C_2 \cdot \nabla F \times \nabla G$. One may immediately verify that this bracket—which is essentially a "Nambu" bracket[12]—indeed defines a Poisson bracket on $\mathbb{R}^3$. (That is, the bracket is a bilinear, skew-symmetric operation satisfying both the Jacobi identity and the Leibnitz rule for derivation of a product.) However, the $\mathbb{R}^3$ Poisson bracket is degenerate, since $\{C_2, G\} = 0$ for every $G(\mathbf{x})$. The function C_2 is said to be the "Casimir function" for this $\mathbb{R}^3$ Poisson bracket. In terms of this bracket, Eq. (13) acquires the Hamiltonian form $\dot{\mathbf{x}} = \{\mathbf{x}, C_1\}$. Hence Eq. (13) is Hamiltonian on $\mathbb{R}^3$ with Hamiltonian function C_1 and Casimir function C_2 for this noncanonical Poisson bracket. Clearly, the roles of C_1 and C_2 could be reversed. Indeed, restricting to a level surface of either C_1 or C_2 reduces the problem to a one degree of freedom Hamiltonian system with the usual symplectic Poisson bracket. All such systems are integrable. Thus Eq. (13), representing either the Chandrasekhar flow with $K = 0$, or the Arter flow with $b = 0$, is an integrable Hamiltonian system. Furthermore, the Arter flow with $b \neq 0$ is expressible as

$$\dot{\mathbf{x}} = \nabla C_1 \times \nabla C_2 + b \nabla C_1' \times \nabla C_2', \tag{14}$$

where

$$\begin{aligned} C_1' &= \log[\sin(x+y)/\sin(x-y)],\\ C_2' &= \sin(x+y)\sin(x-y)\sin(2z).\end{aligned} \tag{15}$$

Hence the Arter flow is the sum of two integrable Hamiltonian flows in $\mathbb{R}^3$, related to each other by a 45° rotation symmetry. This discrete symmetry produces invariant surfaces for the Arter flow in the shape of vertical prisms, whose horizontal cross sections are 45° isoceles triangles. Numerical simulations for both the Arter flow and the Chandrasekhar flow are discussed in the next section.

III. SIMULATION OF THREE-DIMENSIONAL ADVECTION

A. Volume-preserving numerical algorithm

Following Thyagaraja and Haas,[13] Scovel[14] has developed a volume-preserving (and hence helicity-preserving) numerical integration algorithm for divergenceless vector fields in $\mathbb{R}^3$, which we use below to visualize the Arter flow (8) and the Chandrasekhar flow (9). Details of the numerical algorithm can be found in Scovel.[14] Here we give a brief sketch of the algorithm because this is one of its first applications in fluid dynamics. Consider a map $(x,y,z) \to (X,Y,Z)$ represented implicitly by the equations

$$X = f(x,y,Z), \quad Y = g(x,y,Z). \quad z = h(x,y,Z). \tag{16}$$

(This is akin to using old and new phase-space variables in the generating function for a canonical transformation in

Downloaded 07 Jan 2004 to 128.165.156.80. Redistribution subject to AIP license or copyright, see http://ojps.aip.org/phf/phfcr.jsp

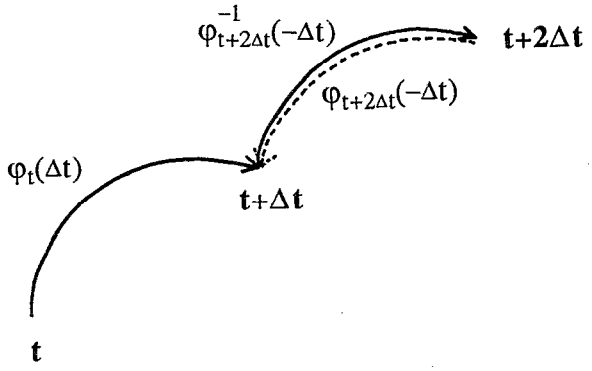

FIG. 1. Illustration of the second-order volume-preserving integrator.

classical mechanics.) Requiring $dX\,dY\,dZ = dx\,dy\,dz$ shows that the map (16) is volume preserving, if and only if,

$$\frac{\partial h}{\partial Z} = \frac{\partial f}{\partial x}\frac{\partial g}{\partial y} - \frac{\partial f}{\partial y}\frac{\partial g}{\partial x}. \tag{17}$$

This relation determines h as the partial integral with respect to Z of the x-y Jacobian of the two generating functions f and g. Now, let $\mathbf{v} = (v_1, v_2, v_3)$ be a divergenceless vector field. Approximating the flow map of this vector field as a function of t, and matching coefficients to determine f and g, gives

$$X = x + tf_1(x,y,Z), \quad Y = y + tg_1(x,y,Z),$$
$$z = Z + th_1(x,y,Z) + t^2 h_2(x,y,Z),$$

where

$$f_1 = v_1, \quad g_1 = v_2, \quad h_1 = -v_3$$

and

$$h_2 = \int^Z v_{1,x}v_{2,y} - v_{1,y}v_{2,x}\,dZ. \tag{18}$$

Denote by $\varphi(t)$, the resulting map $(x, y, z) \to (X, Y, Z)$. The map $\varphi(t)$ is first-order accurate and volume preserving to within the accuracy to which the implicit equations are solved. In the following numerical examples, Picard iteration has been terminated upon convergence to within one part in 10^{-12}. Composing two of these first-order maps pro-

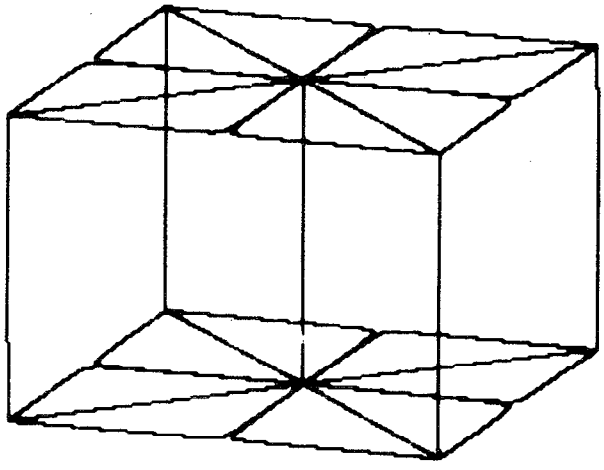

FIG. 2. The fundamental cubic cell of the flow in Eq. (13) is $\{x,y,z|0 \leq |x| + |y| \leq \pi, 0 \leq z \leq \pi\}$.

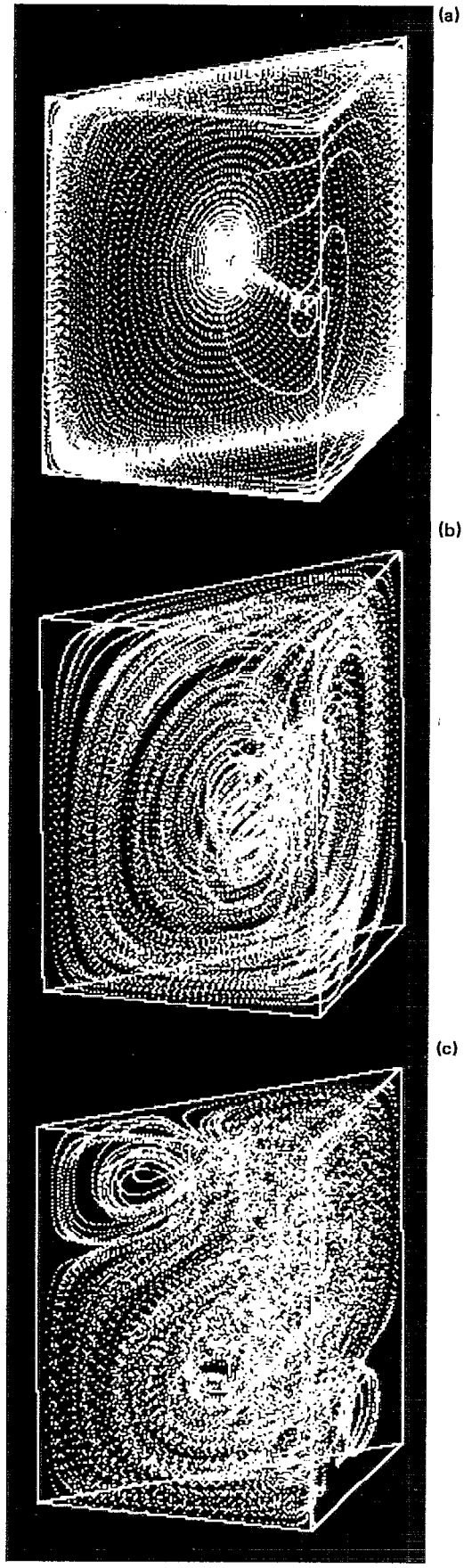

FIG. 3. Arter flows with three different values of the parameter b: (a) $b = 0.03$, (b) $b = 0.3$, and (c) $b = 1.0$

Downloaded 07 Jan 2004 to 128.165.156.80. Redistribution subject to AIP license or copyright, see http://ojps.aip.org/phf/phfcr.jsp

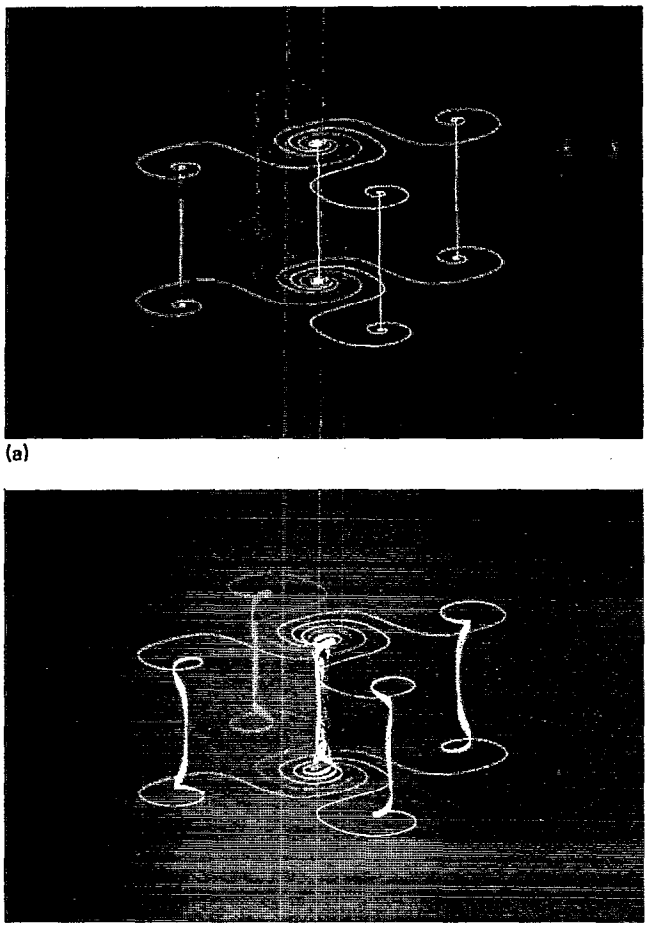

FIG. 4. Chandrasekhar flows with $K = 2$. The initial positions of the particles are: (a) in the plane $z = 0$; and (b) slightly above the plane $z = 0$.

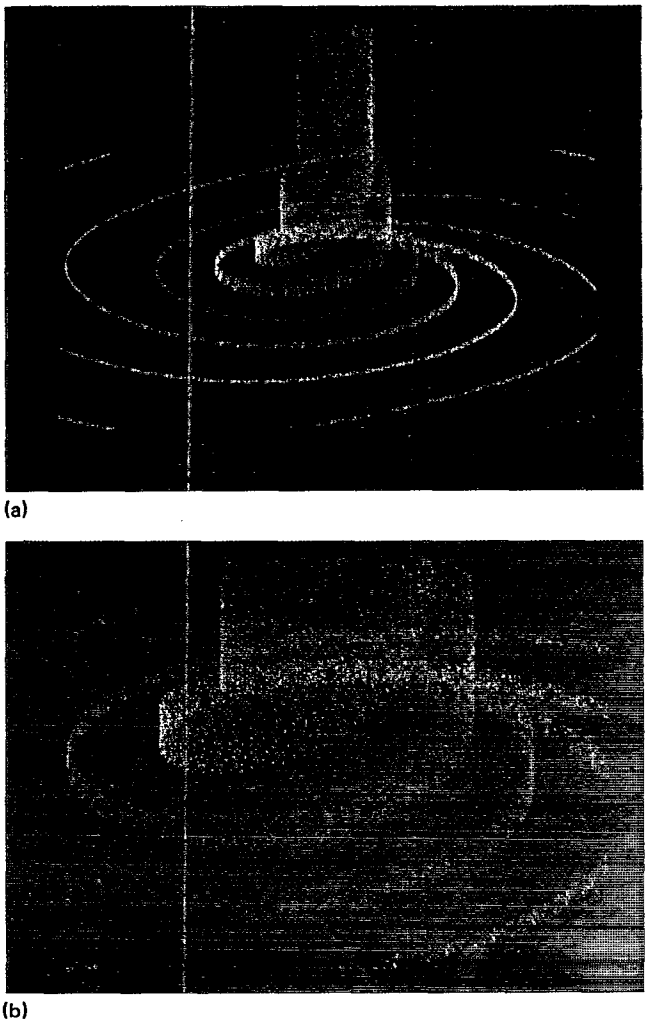

FIG. 5. Two magnified views of Fig. 4 (b), showing the ribbons in the vicinity of the saddle focus.

duces the map sketched in Fig. 1, $\psi(2t) = \varphi^{-1}(-t)\cdot\varphi(t)$, which is volume preserving and *second-order* accurate [since the first-order map $\varphi(t)$ satisfies to second-order accuracy the group property $\varphi^{-1}(t)\cdot\varphi(t) = \text{identity}$].

Explicitly, we use the following second-order volume-preserving integrator, $(x_0,y_0,z_0;t) \to (x_1,y_1,z_1;t+\Delta t) \to (x_2,y_2,z_2;t+2\,\Delta t)$, which also *preserves the helicity of the flow*,[14]

$$
\begin{aligned}
x_1 &= x_0 + \Delta t f_1(x_0,y_0,z_1;t),\\
y_1 &= y_0 + \Delta t g_1(x_0,y_0,z_1;t),\\
z_0 &= z_1 + \Delta t h_1(x_0,y_0,z_1;t) + (\Delta t)^2 h_2(x_0,y_0,z_1;t),
\end{aligned}
\tag{19}
$$

$$
\begin{aligned}
x_1 &= x_2 - \Delta t f_1(x_2,y_2,z_1;t+2\,\Delta t),\\
y_1 &= y_2 - \Delta t g_1(x_2,y_2,z_1;t+2\,\Delta t),\\
z_2 &= z_1 - \Delta t h_1(x_2,y_2,z_1;t+2\,\Delta t)\\
&\quad + (\Delta t)^2 h_2(x_2,y_2,z_1;t+2\,\Delta t).
\end{aligned}
\tag{20}
$$

(Notice that this algorithm would also apply to time-dependent flows, upon regarding the time variable t as a parameter.)

B. Arter and Chandrasekhar flow simulations

We now concentrate on the Arter and Chandrasekhar flows, and show the results of numerical simulations using the volume preserving integrator for several parameter values in each case. Figure 2 shows the fundamental cubical cell $(0 \leqslant |x| + |y| \leqslant \pi, 0 \leqslant z \leqslant \pi)$ of the basic flow (13), which may be regarded as the "unperturbed version" of both of these flows. The planes $x = 0, y = 0$ are invariant surfaces. (In Fig. 2, two closed trajectories are shown in the plane $y = 0$, $x < 0$.) The points $x = 0, \pm\pi, y = 0, \pm\pi$, and $z = 0, \pi$ are 1–2 saddle-focus points, with heteroclinic connections between $z = 0$ and $z = \pi$. The lines of intersection of the planes $x = \pm\pi/2$ and $y = \pm\pi/2$ with the horizontal midplane $z = \pi/2$ are sets of (neutrally stable) fixed points.

Arter flows with different values of b are shown in Figs. 3(a)–3(c). [Figure 3(a): $b = 0.03$; Fig. 3(b): $b = 0.3$; and Fig. 3(c): $b = 1.0$.] The fundamental cubical cell is composed of eight triangular prisms. (Namely, the basic prism $0 \leqslant x \leqslant \pi/2$, $x \leqslant y \leqslant \pi - x$, $0 \leqslant z \leqslant \pi$, and its reflections across the planes $x = 0$, $y = 0$, $x + y = 0$, and $x - y = 0$.) These prisms are each preserved for Arter flows with any value of b. As b increases, Figs. 3(a)–3(c) show the Arter flows becoming more and more dispersed in the prism (but not tangled; remember this flow has zero helicity). This dispersion, seen as punctures of phase trajectories through a horizontal plane through the midpoint of the cube, is claimed in Ref. 6

Downloaded 07 Jan 2004 to 128.165.156.80. Redistribution subject to AIP license or copyright, see http://ojps.aip.org/phf/phfcr.jsp

to show chaos resulting from resonance-island overlap. At $b = 0.5$, a multiple pitchfork bifurcation occurs in the Arter flow, leading to an even more complex flow shown in Fig. 3(c).

The Chandrasekhar flows (9) for $K \neq 0$ have the same fixed points as for $K = 0$, but the basic cell shape of the flow is no longer cubical. Figure 4 shows particle trajectories for the Chandrasekhar flows with $K = 2$. As shown in Fig. 4, these flows follow three-dimensional dynamics near a periodic network of saddle-focus heteroclinic connections with discrete four-fold symmetry under rotations by $\pi/2$. A particle started at a point in the plane $z = 0$ spirals with rotation frequency K into the (x,y) origin, then rises along the z axis up to the horizontal plane $z = \pi$, whereupon it spirals outward in one sense, reaches an inflection point, and then spirals inward in the opposite sense into another spiral focus in the same plane. Thereafter, the particle falls along the z direction until it reaches the $z = 0$ plane, where it again spirals outward and returns through its initial position. On each of the horizontal planes $z = 0$ and $z = \pi$, there is a square array of interconnected saddle-focus points, and the planes at $z = 0$ and $z = \pi$ are connected by heteroclinic orbits through those saddle focus points. Each saddle focus in this heteroclinic network satisfies the Shilnikov criterion.[15] So one would be tempted to conjecture that the perturbations introduced by numerical error would, in general, produce three-dimensional Shilnikov chaos. This is likely, though it has not been proven for the numerical algorithm we use here. Particles started at points slightly off the planes of $z = 0$, π tend to stay in thin, ribbon-shaped regions in curly sheets with opposite handed twists at $z = 0$ and $z = \pi$ [see Fig. 5(a)]. In Fig. 5(b), we see how the ribbons from different initial positions entangle themselves around the axes. Numerical results from the volume-preserving integrator show intricate patterns in these ribbons as a result of the phase relations imposed upon near-recurrence orbits by conservation of volume in the numerical scheme. Without the small errors introduced by numerical approximation, the near recurrences seen in the numerical integrations of the Chandrasekhar flow in Fig. 5 would be exact periodic orbits. The process of braiding and unbraiding, tangling and untangling of these orbits induced in the vicinity of the saddle foci by perturbations of the Chandrasekhar flow is a topic for future study.

ACKNOWLEDGMENTS

We are grateful to J. C. Scovel for fruitful discussions of his volume-preserving algorithm and to G. Kovacic for helpful remarks leading to discovery of the bifurcation at $b = 0.5$ in the Arter flow.

This work was partially supported by DARPA Contract No. AO6630, in Computational and Applied Mathematics Program, and by Grant No. 215 from the University of California, Institute for Geophysics and Planetary Physics.

[1] V. I. Arnold, C. R. Acad. Sci. Paris A **261**, 17 (1965).
[2] V. I. Arnold, Sel. Math. Sov. **5** (4), 327 (1986).
[3] V. I. Arnold, Am. Math. Soc. Transl. **2**, 137, 119 (1986).
[4] M. Hénon, C. R. Acad. Sci. Paris A **262**, 312 (1966).
[5] S. Chandrasekhar, *Hydrodynamic and Hydromagnetic Stability* (Clarendon, Oxford, 1961).
[6] W. Arter, Phys. Lett. A **97**, 171 (1983).
[7] S. Chandrasekhar, Proc. Natl. Acad. Sci. **42**, 1 (1956).
[8] S. Chandrasekhar and K. Prendergast, Proc. Natl. Acad. Sci. **42**, 5 (1956).
[9] S. Chandrasekhar and P. C. Kendall, Astrophys. J. **126**, 457 (1957).
[10] T. Dombre, U. Frisch, J. M. Greene, M. Hénon, A. Mehr, and A. M. Soward, J. Fluid Mech. **167**, 353 (1986).
[11] G. Veronis, J. Fluid Mech. **31**, 113 (1968).
[12] Y. Nambu, Phys. Rev. D **7**, 2405 (1973).
[13] A. Thyagaraja and F. A. Haas, Phys. Fluids **28**, 1005 (1985).
[14] J. C. Scovel, to appear in *Proceedings of the MSRI Workshop on the Geometry of Hamiltonian Systems*, Berkeley, June 1989.
[15] L. P. Shilnikov, Sov. Math. Dokl. **6**, 163 (1965).

Downloaded 07 Jan 2004 to 128.165.156.80. Redistribution subject to AIP license or copyright, see http://ojps.aip.org/phf/phfcr.jsp